Graphene inclusion on Anion-Exchange Membrane Properties for Alkaline Water Electrolyzers

Daniela Ion-Ebrasu[a], Simona Caprarescu[b], Alin Chitu[a], Roxana Trusca[c], Violeta Niculescu[a], Raluca Gabor[d], Elena Carcadea[a], Mihai Varlam[a], Bogdan Stefan Vasile[c], Bruno G. Pollet[e]

[a]National Institute for Cryogenics and Isotopic Technologies ICSI-Rm. Valcea, National Center for Hydrogen & Fuel Cells, Uzinei Str. no. 4, 240050, Ramnicu Valcea, Romania

[b]University Politehnica of Bucharest, Faculty of Applied Chemistry and Materials Sciences, Department of Inorganic Chemistry, Physical Chemistry and Electrochemistry, Bucharest, Romania

[c]National Research Center for Micro and Nanomaterials, Faculty of Applied Chemistry and Materials Science, University Politehnica of Bucharest

[d]National Institute for Research and Development in Chemistry and Petrochemistry, 202 Independentei, 060021 Bucharest, Romania

[e]Department of Energy and Process Engineering, Faculty of Engineering

Norwegian University of Science and Technology (NTNU)

NO-7491 Trondheim, Norway

*Corresponding author: Daniela Ion-Ebrasu; email: daniela.ebrasu@icsi.ro

Highlights

- A simple one-step strategy for the development of graphene composite membranes is described.
- The presence of graphene nanoparticles increases the stiffness of the composite membranes, as well as the thermal stability when compared to pristine commercial FAA3-20® and FAA3-30® membranes from Fumatech.
- The hydroxide ion conductivity increases in the graphene composite membranes with graphene concentration and temperature.

Abstract

The main issues facing the development of Anion Exchange Membranes (AEM) are the low hydroxide ion (OH^-) conductivity compared to protons (H^+) and the thermal and chemical stability. Nowadays, graphene is considered one of the most promising candidates for improving the ionic transport properties, isotopic selectivity and conductivity throughout its unique two-dimensional (2*D*) structure. In this paper, we report on the preparation and characterization of graphene composite membranes and compare their performance with commercial FAA3-20® and FAA3-30® membranes from Fumatech. Various amounts of commercial graphene were incorporated into the Fumion® FAA-3 in NMP (10%), solutions which were then used to fabricate anion exchange membranes (AEMs) by the doctor-blade method. Commercial and graphene-composite AEMs were studied by Fourier Transform Infrared Spectroscopy (FTIR), Thermogravimetric Analysis (TGA) and Differential Scanning Calorimetry (DSC), Scanning Electron Microscopy (SEM), Dynamic Mechanical Analysis (DMA), Water Uptake (WU), Ionic Exchange Capacity (IEC), and Four-points in Plane Impedance Spectroscopy. The results indicated that the composite membranes containing 50 mg of graphene exhibited an improved thermal, mechanical, IEC (3.16 mmol/g) and OH^- conductivity (113.27 mS/cm) at 80 °C under fully humidified conditions (RH = 100%).

Keywords: Graphene; Membrane; Anion-Exchanger; Water Electrolysis

Introduction

Nowadays there are two main commercial water electrolysis technologies that operate at low temperatures, alkaline and proton exchange membranes (PEM) electrolyzers. In the case of alkaline technology, the large inter-electrode distance, absence of dense (membrane) separator and high electrolyte recirculation lead to poor performance and incompatibility under intermittent operations when integrated with renewable energy systems (RES), which renders them inappropriate for renewable electricity storage. Proton exchange membrane water electrolyzers (PEMWEs) exhibit better performance and efficiency than alkaline water electrolyzers (AWE), but they suffer from very poor durability, high cost due to the presence of Platinum Group Metal (PGM)-based catalysts e.g. Pt and Ir (as IrO_2) and proton exchange membranes (PEM) e.g. Nafion® [1-3].

A promising alternative to PEMWEs and AWEs, is the polymer-based anion exchange membrane water electrolyzer (AEMWE) that has the advantage of containing non-precious metal catalysts (NPMC) and less expensive membranes. There are two main differences between PEMWEs and AEMWEs; for example for PEMWEs, protons (H^+, cations) are transferred from the anode to the cathode through the PEM, whereas for AEMWEs, hydroxide ions (OH^-, anions) are transported through the positively charged polymeric membrane from the cathode to the anode [4-6].

AEMWEs are expected to be a game-changer among water electrolysis technologies, as they combine the performance of PEMWEs under less corrosive environment and the robustness of AWEs. Therefore, over the last few years, there has been a growing interest in developing polymer anion exchange membrane (AEM) [7,8].

In comparison with liquid electrolyte, the use of an anion exchange membrane in an alkaline electrolyzer offers many advantages such as: (i) the absence of leaking, (ii) volumetric stability, (iii) ease of handling, (iv) reduction in the size and weight of the electrolyzer, and (v) simpler Balance of Plant (BoP) [9]. Moreover, AEMWEs use low-cost hydroxide transport polymer electrolyte membranes and non-precious metal catalysts (NPMC) instead of the expensive Nafion® and the costly PGM-based in PEMWEs [10-12].

By definition, anion exchange material requires positively charged groups on the polymer backbone to work as membrane or resin in separation or ion exchange processes. If the positive charges are neutralized for whatever reason, the anion exchanger loses its function and becomes inactive. This is a critical current issue with hydroxide ion exchange membranes, in which the highly nucleophilic hydroxide counter ion attacks both the positively charged functional quaternary ammonium (QA) groups and the polymer backbone [13, 14]. Specifically, the cation degradation is considered to be the main reason why the AEMWEs lose performance beyond 60°C. In order to reduce the AEMs degradation at elevated temperature, and to increase the ionic conductivity, several strategies have been attempts during the last decade.

Nowadays, poly-(phenylene oxide) [15, 16], poly-(arylene ether ketone) [1-19] poly-(ether ether ketone) [20], and polystyrene [21] are used to produce AEMWEs through bromomethylation or chloromethylation and consecutive quaternization [22]. In addition, inorganic components were added to the quaternized polymer. For example, titanium dioxide (TiO_2) [23], zirconium dioxide (ZrO_2) [24], aluminium oxide (α-Al_2O_3) [25], bentonite [26], graphene oxide [27, 28] were added to the organic matrix in order to improve morphological stability.

Shin-Cheng Jang *et al.* [29] reported studies about the quaternized chitosan (QCS)/functionalized carbon nanotubes (CNTs) composite anion exchange membranes with different amounts of QCS@CNTs. The membranes were prepared by coating the CNTs with a layer of QCS through noncovalent surface modification and then blending with QCS matrix. The effects of the addition amount of QCS@CNTs led to an improvement of the tensile strength and alkaline stability of the composite membrane with the increase of the addition amount of QCS@CNTs, although the OH^- ion conductivity decreased slightly but could still maintain above 15 mS cm^{-1}, when compared with that of pure QCS membrane.

Omar Movil *et al.* [30] prepared nanocomposite membranes by incorporation of the functionalized graphene oxide (FGO) into polyvinyl alcohol poly-(diallyldimethylammonium chloride) semi-interpenetrating polymer networks (PVA/PDA SIPNs). The results revealed that the composite membrane exhibited the highest value of OH^- conductivity (12.1 mS cm^{-1} @ 30°C and 21 mS cm^{-1} @ 80°C), as well as improved thermo-mechanical stability at 100% RH, with respect to the membrane without FGO filler (7.14 to 9.04 mS cm^{-1} in the temperature range from 30°C to 50°C).

In this study, we report a simple one-step strategy for the development of graphene composite membranes. The *as*-prepared membranes were compared with commercial FAA3-20® and FAA3-30® membranes from Fumatech. The novelty of this method consists on tailoring the anion exchange membrane properties, by incorporating different commercial graphene nanoparticles within the anion exchange polymer solution. Our results showed a decrease of the quaternary ammonium (QA) groups and polymer backbone degradation, and enhancements in the alkaline

stability, mechanical properties, ionic exchange capacity and hydroxide (OH^-) conductivity. In this study, the commercial and graphene-composite AEMs were analyzed by Fourier Transform Infrared Spectroscopy (FTIR), Thermogravimetric Analysis (TGA), Differential Scanning Calorimetry (DSC), Scanning Electron Microscopy (SEM), Dynamic Mechanical Analysis (DMA), Water Uptake (WU), Ionic Exchange Capacity (IEC) and Four-points in Plane Impedance Spectroscopy.

Experimental Methods

2.1. Membranes preparation

Commercial Fumasep® FAA-2-20 and Fumasep® FAA-2-30 anion exchange membranes with 20 µm and 30 µm thickness, respectively, as well as Fumion® solution FAA-3 anion-exchange polymer solution in NMP (10%) concentration weight were purchased from FumaTech BWT GmbH, Germany. The Fumatech membranes and FAA-3 solution are aromatic polymers containing quaternary ammonium functional group, and bromide (Br^-) counterion.

The graphene nanoparticles with surface area of 500 m^2/g were purchased from Alfa Aesar. All other materials were used as received, without further purification. Demineralized water (18.2 MΩ cm) was produced on-site and used for solutions preparation.

The composite graphene modified anion-exchange membranes were prepared by the Doctor blade (or tape casting) method using a COATMASTER 509 MC-I system which was adjusted at a thickness range of 100 µm. Different graphene loadings of 25, 50, 75 and 100 mg, were added to 10 mL Fumion® solution corresponding to 0.25, 0.50, 0.75, 1 w/v % accordingly (Table 1). These

mixtures were then stirred over-night until homogeneous solutions were formed. The solutions were cast onto the Doctor blade glass and the membranes were formed by moving the blade at low speed (5 mm s^{-1}) in order to ensure the formation of uniform composite polymer layers (Figure 1). The same procedure was applied for the ionomer membrane (AEM-Ion) obtained by using the Fumion® solution. The thickness of the membranes was determined from the SEM cross-section images.

Table 1. FAA3 membranes and composite alkaline membranes characteristics

Membranes	**Graphene loading (mg)**	**Graphene concentration (w/v %)**	**Membranes thickness (μm)**
FAA3-20®	-	-	20
FAA3-30®	-	-	30
AEM-Ion	-	-	30
AEMGr0.25%	25	0.25	12
AEMGr0.50%	50	0.50	12
AEMGr0.75%	75	0.75	12
AEMGr1%	100	1	12

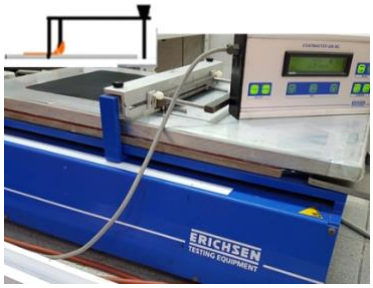

Figure 1. COATMASTER 509 MC-I system used for the fabrication of AEM-composite membranes

2.2 Water Uptake

The water uptake of all the graphene composite membranes samples was determined at 25°C and 50°C. FAA3-20®, FAA3-30®, and AEM-Ion membranes were also used for comparison purposes according with the procedure indicated in another study [20]. The dry membranes that were soaked in water at 25°C and 50°C were weighted before and after soaking. After 24 hours, the samples were wiped off with a clean paper tissue to remove the excess of water, and weight again. Water uptake (*WU*) was calculated using Eq. (1):

$$Wateruptake = \frac{m_{wet} - m_{dry}}{m_{dry}} \times 100 \quad (1)$$

where m_{wet} is the mass of the membrane in after soaking and wiping, and m_{dry} is the is the mass of the dry membrane.

2.3 Ionic exchange capacity (IEC)

The IEC of membranes, that represents the total of active sites or functional groups responsible for ion exchange in polymer electrolyte membrane [31], was determined using the titration method on the membrane in its Cl^- form [32]. The samples of membranes (Br^- form, ~0.1 g) were soaked in 1 M KCl solution (50 mL) for 48 h to obtain the Cl^- form. The excess Cl^- (and K^+) ions were removed

via washing with deionized water for 48 hours. The Cl^- now present as a counterion in the membrane was displaced into a 1.0 M $NaNO_3$ solution (25 mL) for 48 hours. The membranes (Cl^- now present as a counterion in the membrane) were soaked in 0.5 M $NaNO_3$ for 48 hours. The membranes were then washed with deionized water for 48 h. All $NaNO_3$ solutions were titrated with 0.01 M $AgNO_3$, using 3 drops of K_2CrO_4 (5 wt%) as a colorimetric indicator. The membranes were exchanged back to the Cl^- form after titration and dried at 50˚C in a vacuum over for 3 hours to obtain the dry mass (m_{dry}). IEC is expressed as millimoles of Cl^- per gram of dry membrane:

$$IEC(mmolCl^{-1}/g) = \frac{V_{AgNO_3} x C_{AgNO_3}}{m_{dry}} \quad (2)$$

where V_{AgNO3} and C_{AgNO3} are the end-point volume (cm^3) and concentration (M) of the titrant solution, respectively, and m_{dry} is the mass of the dry membrane.

2.4 Hydroxide conductivity and activation energy

The influence of graphene concentration towards hydroxide conductivity was studied at different temperatures in the range of 25 ˚C to 80˚C. In order to ensure transport of the hydroxide (OH^-) through the membranes, the samples were activated in 0.01 M KOH for 48 hours, and washed with deionized water. The hydroxide conductivity measurements were carried out using in-plane direction by AC impedance spectroscopy using a 4-point in-house made conductivity cell, at 100% RH, soaked in 0.01 M KOH (pH=12), by passing a current through two outer electrodes and measuring the voltage through the inner electrodes [33, 34]. In the 4-electrode configuration, there was virtually no current flowing at the inner cell voltage sensing electrodes. Therefore, polarization

did not occur. The resistance (R in Ω) of each sample was determined at the frequency producing the minimum imaginary response. Conductivity was calculated using equation (3):

$$\sigma = \frac{L}{R*w*t} \quad (3)$$

where σ is the conductivity in mS cm^{-1}, R is the *real* part of the impedance in Ω, L is the fixed distance between the two electrodes (3 cm), w is the width of the sample (1.5 cm), and t is the thickness of the membrane in cm (Figure 2). The cell was fabricated on a Stratasys Objet 260 Connex *3D* printer using Rigur RGD450 material, a polyjet simulated polypropylene (PP) that is an alkaline and temperature resistant polymer. The 4 electrodes were made of stainless steel (SS) of 1 mm thickness. The electrochemical impedance (EIS) spectra were recorded at different frequencies from 1 MHz to 0.1 Hz and at a signal amplitude of 100 mV using a Princeton Applied Potentiostat/Galvanostat. Figure 3 shows the membranes mounted in the conductivity cell.

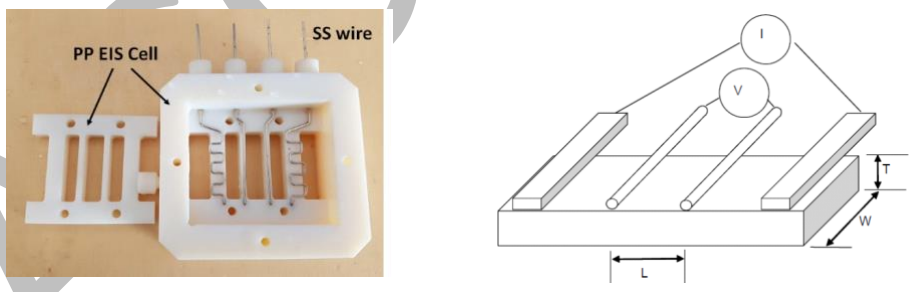

Figure 2. Scheme and picture of the home-made conductivity cell

The activation energy E_a (kJ mol^{-1}) required for hydroxide (OH^-) transfer through the membranes from one free-site to another was calculated using the following *Arrhenius equation* [9, 10].

$$ln\sigma = ln\sigma_0 - \frac{E_a}{RT} \quad (4)$$

Where σ and σ_0 are the conductivity and pre-exponential factor, respectively, in mS cm^{-1}, R is the gas constant (8.314 J mol^{-1} K^{-1}), and T is the absolute temperature in K.

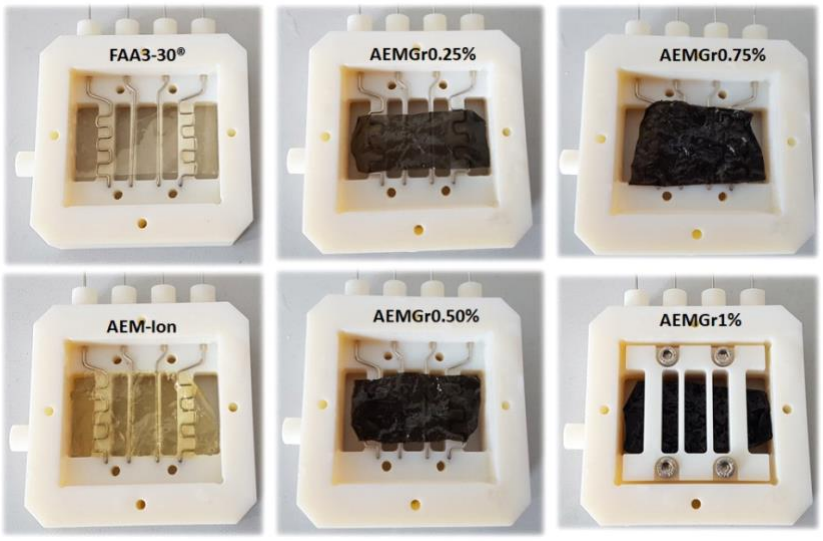

Figure 3. Picture of the membranes mounted in the conductivity cell

2.6 Scanning electron microscopy (SEM) characterization

SEM characterization was carried out by using the Quanta INSPECT F50 system. Prior to SEM analyses, the membranes were broken in liquid nitrogen (N_2) and coated with gold in order to increase samples' electrical conductivity and to obtain the SEM cross-section images.

2.7. Fourier Transform Infrared Spectroscopy (FTIR) Analysis

FTIR characterization of the AEM composite membranes was carried out by the transmittance method at a resolution of 4 cm^{-1} in domain of 400-4,000 cm^{-1}, by using a Frontier FT-NIR spectrometer.

2.8. UV-Vis characterization

The membranes were characterized by ultraviolet–visible spectroscopy (UV–Vis). The spectra were recorded using the SPECORD 200 PLUS Double Beam Spectrophotometer from Analytik Jena, Germany, in the wavelength range of 300 to 1,000 nm. In order to confirm incorporation of the graphene nanoparticles in the polymer matrix, the related spectra were compared with those collected for the FAA3-20®, FAA3-30®, and AEM-Ion membranes.

2.9 Thermogravimetric analysis (TGA) and differential scanning calorimetry (DSC)

Thermogravimetric analysis (TGA) and glass transition (T_g) characterizations by differential scanning calorimetry (DSC) of the membranes (sample mass: ~10 mg) were carried out using a TGA-DSC e NETZCH STA 449 F5 Jupiter, in the temperature range of 25°C - 800°C at a heating rate of 10°C min^{-1} under nitrogen (N_2) flow.

2.10 Dynamic Mechanical Analysis (DMA)

Dynamic Mechanical Analysis (DMA) were performed in the temperature range of *RT* to 40°C using a clamp tension for films on films with length 12.75-12.85 mm; width 6.8 mm and thickness 0.01-0.05 mm at 1 Hz frequency oscillation, strain 0.1 and static force 0.08 settings, in air bearing gas and in temperature ramp method. The storage modulus (MPa) was plotted against time.

3. Results and Discussions

3.1. *Water Uptake (WU) and Ionic Exchange Capacity (IEC)*

The water content by Water Uptake (WU) and the Ionic Exchange Capacity (IEC) are related to the ion conductivity due to the fixed ion exchange sites in the membrane. However, this relationship is not always true for composite membranes because of incorporation by dispersion of graphene nanoparticles within the polymer matrix, that creates interconnected channels full of electrolyte solution (water, different concentration of KOH). In the case of AEMs, these channels increase the hydroxide ion (OH^-) transfer from one positive QA to the next one, which in turn increase OH^- conductivity.

Table 2 shows the WU and IEC results. From the WU experiments carried out at 25°C, it can be observed a slight improvement in WU and IEC data for membranes containing graphene, but this observation was not observed at 50°C probably due to the change in the morphology and thickness of the AEMs when temperature increased [21]. From our experiments, it was observed that the IEC of the composite AEMs was improved with graphene concentration up to 3.16 mmol/g, corresponding to 0.50 w/v %. Increasing the graphene loading led to a decrease in IEC probably due to the reduction of the free ionic groups with the number of carbon nanoparticles. These results could be probably due to the membranes' structure and by the thermal and mechanical behaviour. This is the subject of our next investigation which is presented further on.

Table 2. FAA3 membranes and composite alkaline membranes Water Uptake (WU) and Ionic Exchange Capacity (IEC)

Membranes	Water uptake (%)		(IEC)
	25°C	50°C	(mmol/g)
FAA3-20®	15.6	23.53	1.88
FAA3-30®	16.2	37	1.6
AEM-Ion	13.56	32	1.72
AEMGr0.25%	15.33	21.43	2.75
AEMGR0.50%	18.46	21.89	3.16
AEMGr0.75%	16	19.50	2.18
AEMGr1%	15.71	18.98	2.21

3.1 Hydroxide conductivity and activation energy

It is well-known that the water content influences to a large extent the ionic conductivity behaviour of the membranes [36]. However, in the case of composite membranes, this dependency is not necessarily true, especially at temperatures higher than temperatures (50°C and more). Figure 4 (a) shows the hydroxide ion conductivity of the membranes in the temperature range of 25°C to 80°C in 0.01 M KOH (pH = 12) under fully humidified conditions (RH = 100%). Values are summarized in Table 3. The data show that FAA3-30® is stable up to 55 °C, FAA3-20® is stable up to 60°C, and AEM-Ion can be measured up to 75°C. It was found that the OH^- conductivity for all samples increased with temperature. Moreover, the FAA3-20® conductivity (26.88 mS cm^{-1}) measured at 25°C is in good agreement with the one reported by Aricò *et al.* (30 mS cm^{-1} in water

at 25°C) [37]. It was observed that the inclusion of different quantities of graphene in the ionomer solution decreased the transport barrier for OH^- anions and increased the ionic conductivity, and enhanced the alkaline solution stability of the composite membranes. For example, at a temperature of ca. 80°C, a value of 113.27 mS cm^{-1} corresponding to 0.50 w/v % of graphene can be achieved. This value corresponds to an activation energy E_a of 4.72 kJ/mol. E_a for all the membranes was calculated by using the *Arrhenius equation* (Eq. 4*)* represented in Figure 4(b). From the linear plots, the intercept ($ln\sigma_0$) and the slope ($1/T\ 10^3 (K^{-1})$) could be determined. Here, the slope is equal to ($-E_a/R$) and from this relationship, the activation energy for all the membranes can be determined.

The hydroxide ion conductivity as well as the E_a values are in very good agreement with *IEC* values, clearly indicating that OH^- conductivity increases with graphene loading up to 50 mg. It is likely that graphene interacts with the polymer matrix through hydrogen bonding and forms additional nano-confined channels that create supplementary pathways for hydroxide ions to be transported through the reverse-Grotthus mechanism. In this case, proton jumps from one water molecule to the nearest OH^- ion, creating a new water molecule and forming a new OH^- ion that is transferred through the composite AEM membrane [38-41]. Thus, this finding could explain the enhancement of the hydroxide ion conductivity and thermal stability for the obtained composite AEMs, compared with the one in the absence of graphene. It is worth noting that increasing the graphene may limit the mobility of the conductive ions and hindering and disrupting the hydroxide ion pathway through the membrane [42-44]. For example, in our conditions, gradual reduction in OH^- conductivity for graphene concentration higher than 0.50 w/v % was observed.

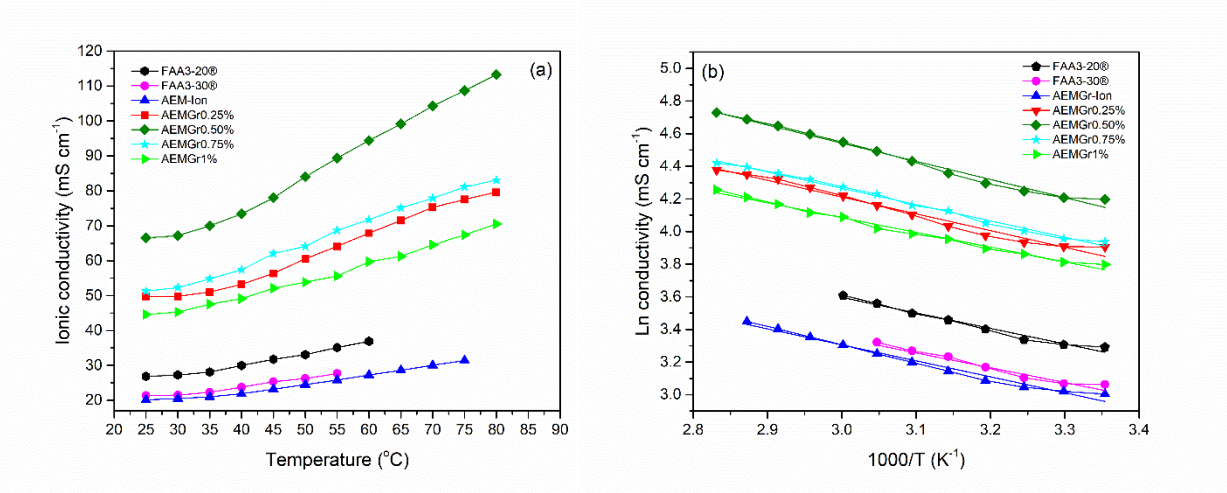

Figure 4. (a) Hydroxide conductivity and, **(b)** *Arrhenius* plot for the FAA3 and composite alkaline membranes

Table 3. Hydroxide conductivity and activation energy (E_a) in domain of 25 °C to 80 °C

Membranes	**Hydroxide conductivity σ (mS/cm)**						**Activation energy E_a (kJ/mol)**
	25 °C	**50 °C**	**55 °C**	**60 °C**	**75 °C**	**80 °C**	
FAA3-20®	26.88	33.07	35.14	36.92	-	-	3.60
FAA3-30®	21.38	26.27	27.70	-	-	-	3.32
AEM-Ion	20.16	24.50	25.78	27.25	31.43	-	3.44
AEMGr0.25%	49.70	60.54	64.12	67.91	77.51	79.64	4.37
AEMGR0.50%	66.52	84.05	89.35	94.40	108.68	113.27	4.72
AEMGr0.75%	51.26	64.12	68.66	71.73	81.07	83.03	4.41
AEMGr1%	44.61	53.83	55.57	59.68	67.37	70.50	4.25

3.3. Scanning electron microscopy (SEM) characterization

The thickness of the composite membranes was determined by cross-sectional measurements using a scanning electron microscopy (SEM). From the cross-sectional views presented in Figure 5, it is evident that the membranes are dense, uniform and without pores. The top-view morphology of the membranes shown in the left-hand side of each SEM picture, indicate that the roughness of the composite membranes increased with graphene loading, the surface was uniform, and no cracks were observed. These observations could be due to the uniform distribution and dipole-dipole interaction between the graphene and ionomer solution.

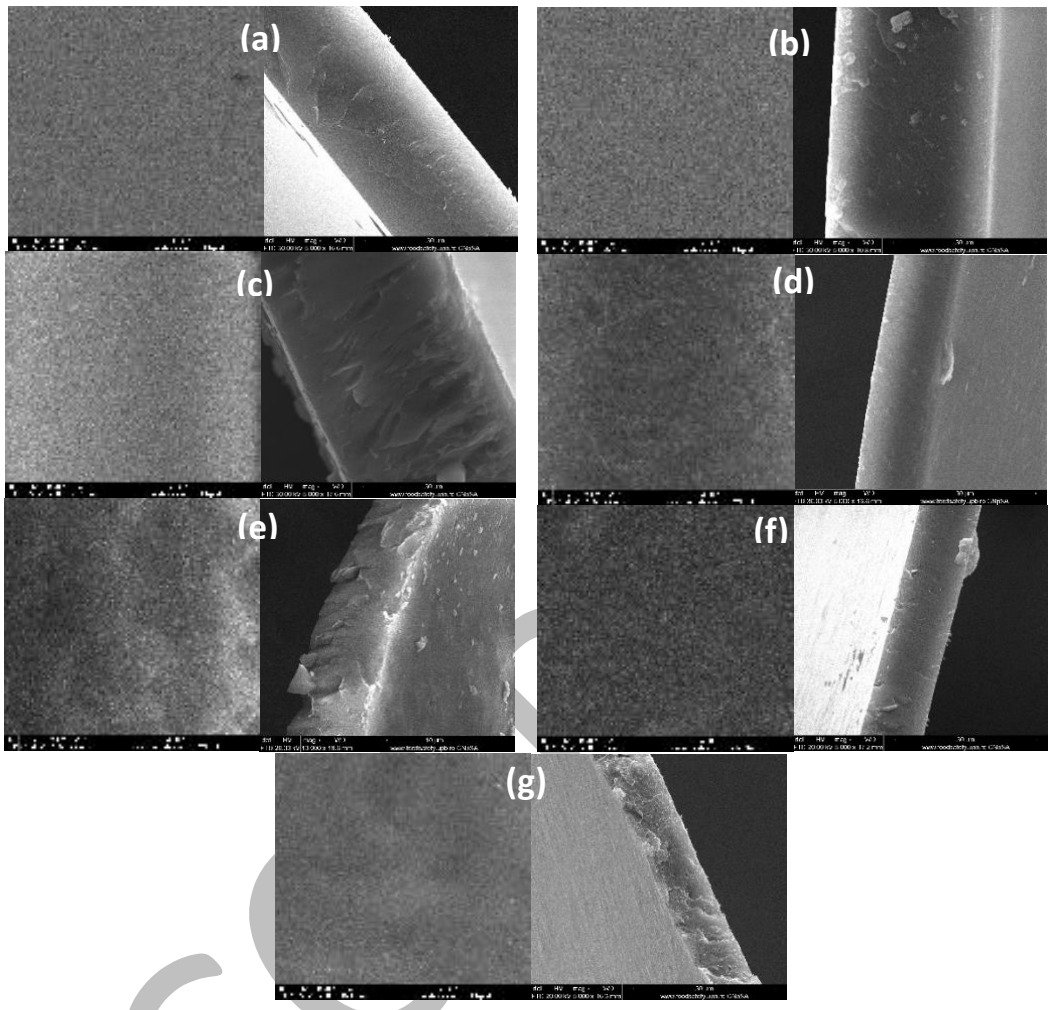

Figure 5. Top-view (left) and cross-section (right) morphology of the **(a)** FAA3-20®; **(b)** FAA3-30®; **(c)** AEM-Ion; **(d)** AEMGr0.25%; **(e)** AEMGr0.50%; **(f)** AEMGr0.75%; **(g)** AEMGr1%

3.4. FTIR Analysis

Overlaid FTIR spectra of all membranes are presented in Figure 6. The broad absorption at 3,100–3,700 cm^{-1} is associated with O-H stretching vibration, and the bands in the region of 2,700–3,100 cm^{-1} are attributed to C-H symmetric and asymmetric stretching O-H groups. The finger-print region shown in Figure 6(b) is useful for detailed FTIR analysis from which are noticed the

characteristic peaks of $–CH_2Br$ located at 1,078 cm^{-1} and 650 cm^{-1} attributed to the stretching and bending vibration from the bromide [21]. 1,025 cm^{-1} and 866 cm^{-1} correspond to C-H in-plane bending and out-of-plane C-H bending vibrations respectively, from the aromatic rings. The absorption peaks at 1,466 and 1,602 cm^{-1} are due to the stretching vibration of N-C bonds in the QA (quaternary ammonium) groups ($–N^+(CH_3)_3$) [9]. The peak at 1,671 cm^{-1} can be assigned to the vibration of $=CH_2$ bending from the aromatic rings [45]. In all studied composite membranes, an increase in absorbance with increased graphene loading was observed, suggesting a successful inclusion of graphene into the AEM polymer and homogenous composite membrane formation due to the interaction between the graphene with the ionomer solution through the hydrogen-bonding.

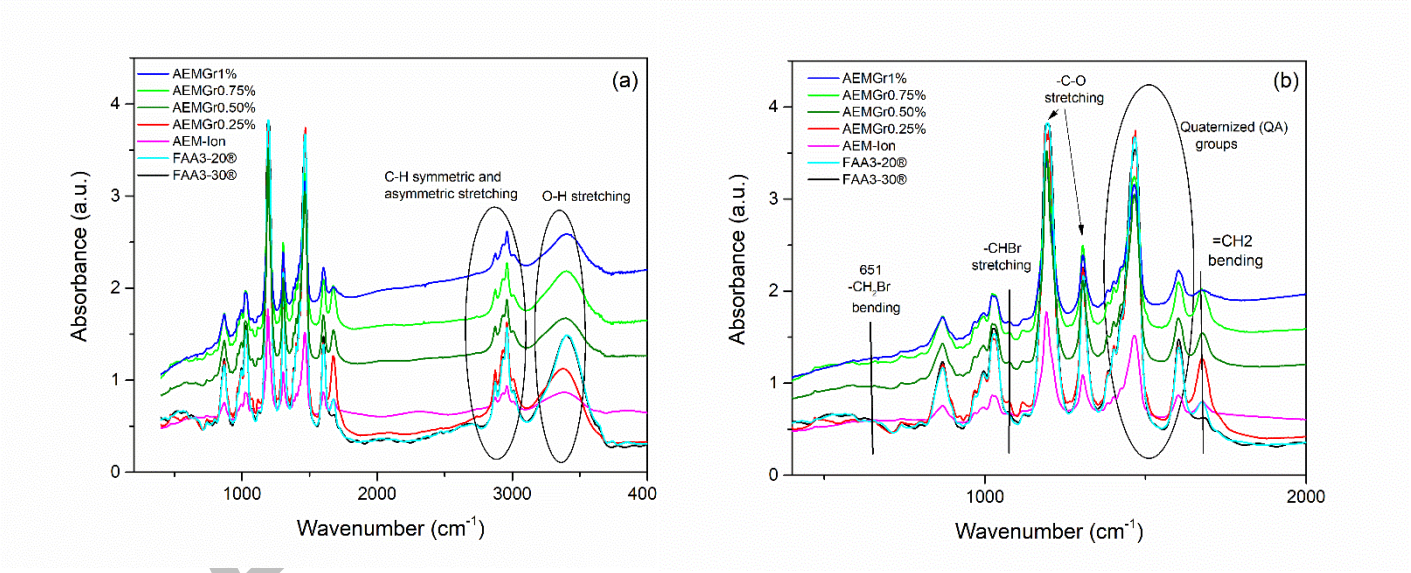

Figure 6. Overlaid FTIR spectra of membranes in domain of **(a)** 400-4000 cm^{-1}; **(b)** finger-print region 400 cm^{-1} – 2,000 cm^{-1}

3.5. UV-Vis characterization

The optical properties of the commercial membranes, AEM-Ion and obtained composite membranes were investigated by UV–Vis spectroscopy (Figure 7). Figure 7 shows the UV-Vis transmission spectra of graphene-anion polymer composite films with a thickness of about 12 μm determined from the cross-sectional SEM image (Fig. 5). In this figure, the transmittance spectra of the commercial and AEM-Ion membranes are also shown for comparison purposes. The analysis of the spectra demonstrates that the transmission decreases due to the incorporation of graphene in the ionomer matrix. It can be observed that the optical scattering of FAA3-20®, FAA3-30® and AEM-Ion graphene occurs in the range of 400-600 nm, and after incorporating graphene in the ionomer, the transmission decreases. Moreover, the composite membranes present (see inset of Figure 7) two types of characteristic features: the first is an optical scattering in the range of 300-400 nm that is characteristic of graphene interaction π-π* transition of the aromatic C-C bond that shifted (right) with an increase in graphene loading [39,40]. The second one in the range of 400-600 nm which is caused by n-π* transitions of the C-O bond and graphene insertion into the polymer matrix.

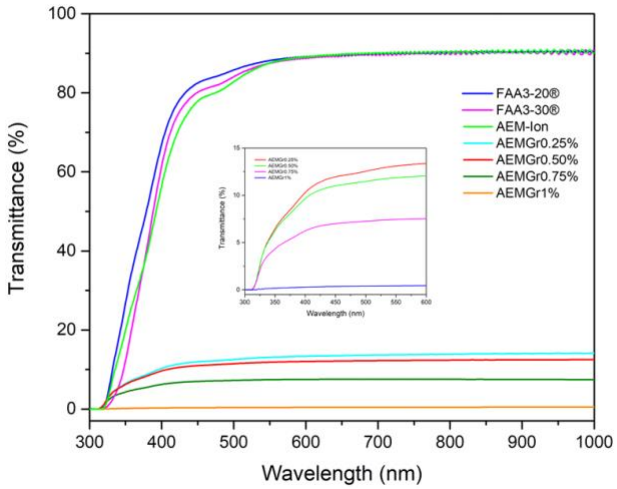

Figure 7. UV-Vis spectra of membranes in domain of 300-1000 nm

3.6 Thermogravimetric analysis (TGA) and differential scanning calorimetry (DSC)

The thermal decomposition curves of the membranes are shown in Figure 8, and the resulted values are presented in Table 4. From the figure, two steps can be observed, the first step from room temperature (*RT*) to 155 °C and the second between 165 °C to 350 °C which are assigned to the loss of the physically and chemically absorbed water in the membranes, and to the degradation of the QA groups, respectively [21,45]. The mass loss in the temperature range of 350°C to 450°C can be ascribed to the wt% of CH_2Br groups [47]. It can be noticed that for the composite membranes with graphene concentration higher than 0.25 w/v %, this step is not present. This observation could be presumably due to the reaction between the graphene and the polymer cation. The absence of this mass loss step in the AEMGr0.50%, AEMGr0.75% and AEMGr1% profile in the temperature range of 350°C to 450°C suggests that these membranes are more thermally stable than the other ones. The mass loss at temperatures higher than 450°C is caused by the decomposition of the polymer backbones.

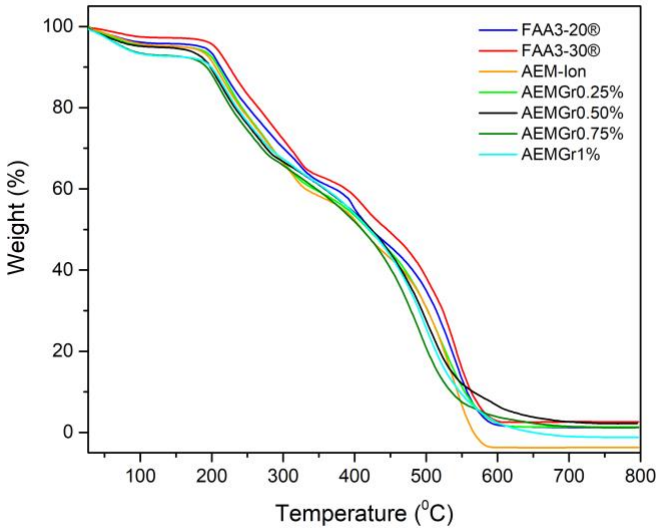

Figure 8. TGA plots of all membranes in the temperature range of of *RT*-800 °C

Table 4. FAA3 membranes and composite alkaline membranes characteristics

Membranes	**TGA (%)**				***Tg* (°C)**
FAA3-20®	3.7	34.8	13.8	46.00	206
FAA3-30®	2.7	34.7	11.7	47.5	207
AEM-Ion	4.2	37.8	12.9	48.2	208
AEMGr0.25%	4.7	36.7	12.1	44.9	209
AEMGr0.50%	4.5	35.1	57.6		212
AEMGr0.75%	6.8	34.7	56.9		213
AEMGr1%	6.5	32.8	61.1		214

The effect of graphene addition into the ionomer solution on the glass transition temperature (T_g) was investigated by DSC as shown in Figure 9. It was found that the presence of graphene nanoparticles increases the stiffness of the polymer which was manifested by the enhancement of

the T_g with increased graphene loadings. This finding could be due to the result of the well dispersed large surface area (SA = 500 m^2/g) graphene nanoparticles causing strong interfacial interactions between the graphene and the polymer matrix, and substantially influencing the thermal and mechanical properties of the membrane [48]. These results can also be correlated with the improvement of the hydroxide ion conductivity of the composite membranes and demonstrate the successful incorporation of the graphene nanoparticles into the Fumion® solution.

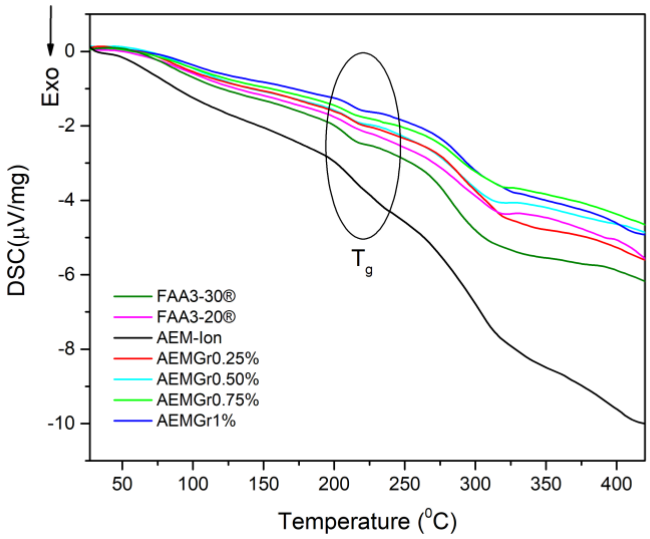

Figure 9. DSC curves of FAA3 and composite alkaline membranes

3.7 Dynamic Mechanical Analysis (DMA)

Figure 10 shows the dynamic thermomechanical response of all membranes i.e. the storage modulus over time (40 min) at an isothermal temperature (40 °C) (a change of the storage modulus over 40 minutes). Usually, the dynamic mechanical properties are directly related to chemistry, therefore, the DMA results presented in Figure 10(a) show that the most stable samples are the commercial membranes [48-50]. However, graphene functionalities increase stiffness of the

composite membranes in comparison with the AEM-Ion (Figure 10(b)), causing an increase in storage modulus. These results further confirm that by using graphene as filler for anion solution, it is possible to produce alkaline exchange membranes with better thermal and mechanical stability.

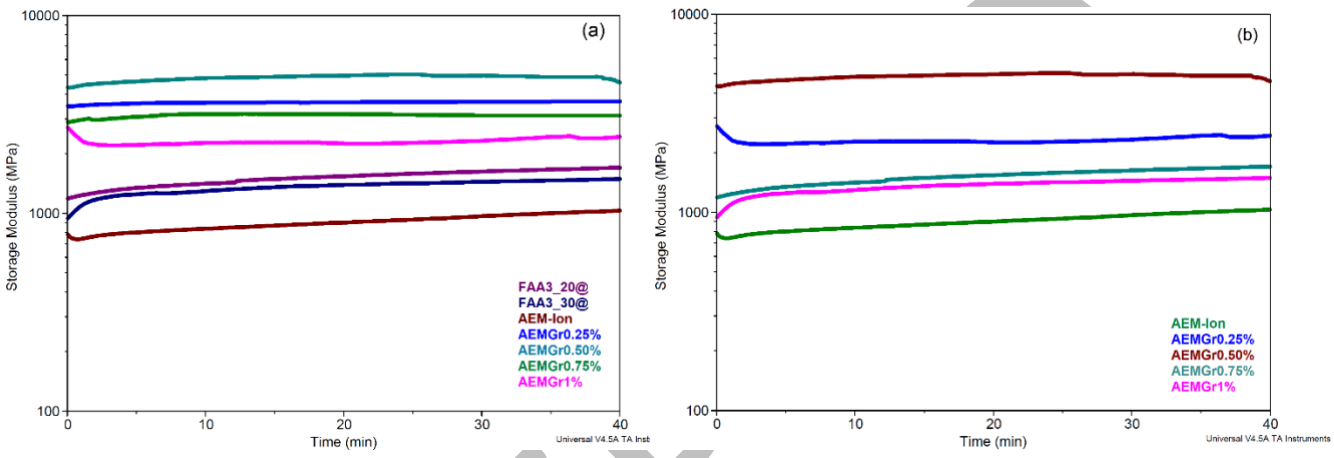

Figure 10. Dynamic thermomechanical response for **(a)** the FAA3 and composite alkaline membranes; **(b)** AEMs composite membranes

Conclusions

Composite graphene modified AEM membranes were successfully developed *via* a simple method of mixing graphene at various loading with Fumion FAA-3-SOLUT-10 ionomer. The structural characterization experiments highlighted that the fabrication of the composite membranes was possible. Electrochemical, thermal and mechanical characterization of the composite membranes showed an improved behaviour when compared to pristine Fumasep® FAA3 membranes. It was found that the hydroxide ion conductivity increased with graphene concentration and temperature due to the unique *2-D* structure of graphene that changes the ion conducting mechanism. The hydroxide ion conductivity results indicated that the conductivity values decreased for the AEMGr0.75% and AEMGr1% membranes, suggesting that the excess amount of graphene could

hinder/disrupt the continuity of ion conduction pathways in the composite membrane. The improved electrochemical, thermal and mechanical properties of the composite AEMs based upon graphene inclusion into the anion-exchange polymer solution, are the basis for future investigations. These membranes will be used for both electrolyzer and fuel cells tests, and the results will be reported in a follow-up paper.

Funding: This study was supported by the Romanian National Authority for Scientific Research & Innovation (Contract 117/16.09.2016), and Romanian Research and Innovation Ministry-Nucleaus Programm (Contract PN19110205/2019).

Acknowledgments: The SEM analyses on samples were possible due to EU-funding grant POSCCE-A2-O2.2.1-2013-1/Priority direction 2, Project No. 638/12.03.2014, cod SMIS-CSNR 48652.

References

[1] A. Ursua, L.M. Gandia, P. Sanchis. Hydrogen production from water electrolysis: current status and future trends, Proceedings of the IEEE, 100 (2) (Feb 2012), p. 410-426.

[2] Marini S, Salvi P, Nelli P, Pesenti R, Villa M, Berrettoni M, et al. Advanced alkaline water electrolysis. Electrochim. Acta. 2012;82:384-391. https://doi.org/10.1016/j.electacta.2012.05.011

[3] Carmo M, Fritz DL, Mergel J, Stolten D. A comprehensive review on PEM water electrolysis, Int J Hydrogen Energy 2013;38:4901-34. https://doi.org/10.1016/j.ijhydene.2013.01.151

[4] Garcia-Vasquez W, Ghalloussi R, Dammak L, Larchet C, Nikonenko V, Grande D. Structure and properties of heterogeneous and homogeneous ion-exchange membranes subjected to ageing in sodium hypochlorite. J Membr Science 2014;452:100-16. https://doi.org/10.1016/j.memsci.2013.10.035

[5] Kumar R, Xu C, Scott K. Graphite oxide/Nafion composite membranes for polymer electrolyte fuel cells. RSC Advances. 2012;2:8777–82. https://doi.org/10.1039/C2RA20225E

[6] Kim AR, Vinothkannan M, Yoo DJ, Sulfonated fluorinated multi-block copolymer hybrid containing sulfonated(poly ether ether ketone) and graphene oxide: A ternary hybrid membrane architecture for electrolyte applications in proton exchange membrane fuel cells. J Energy Chem 2018;27:1247–60, https://doi.org/10.1016/j.jechem.2018.02.020

[7] Schalenbach M, Tjarks G, Carmo M, Lueke W, Mueller M, Stolten D. Acidic or alkaline? Towards a new perspective on the efficiency of water electrolysis. J Electrochem Soc 2016;163: 3197-3208. doi:10.1149/2.0271611jes

[8] Bessarabov D, Millet P. In Chapter 2 Brief Historical Background of Water Electrolysis. In PEM Water Electrolysis, Volume 1, Series Editor. Pollet, B.G., Academic Press is an imprint of Elsevier Ltd., United Kingdom, p. 17-42.

[9] Wu X, Scott K. A polymethacrylate-based quaternary ammonium OH^- ionomer binder, for non-precious metal alkaline anion exchange membrane water electrolysers, J Power Sources 2012; 24:124-9. https://doi.org/10.1016/j.jpowsour.2012.03.069

[10] Vincent I, Bessarabov D. Low cost hydrogen production by anion exchange membrane electrolysis: A review. Renew Sustain Energy Rev 2018;81:1690-1704. https://doi.org/10.1016/j.rser.2017.05.258

[11] Pavel CC, Cecconi F, Emiliani C, Santiccioli S, Scaffidi A, Catanorchi S. et al. Highly efficient platinum group metal free based membrane-electrode assembly for anion exchange membrane water electrolysis. Angew Chem Int Ed Engl 2014;53(5):1378-81. https://doi.org/10.1002/anie.201308099

[12] Vincent I, Bessarabov D. Hydrogen Production by water Electrolysis with an Ultrathin Anion-exchange membrane (AEM). Int J Electrochem Sci 2018;13:11347–58. https://doi:10.20964/2018.12.84 [13] Anion exchange membranes for fuel cells and flow batteries: Transport and stability of model systems Dissertation an der Universit¨at Stuttgart von Michael Giuseppe Marino Max-Planck-Institut fur Festk¨orperforschung 2015, pp 27.

[14] Dongyang C, Hickner MA. Degradation of imidazolium- and quaternary ammonium-functionalized poly(fluorenyl ether ketone sulfone) anion exchange membranes. ACS Applied Materials & Interfaces 2012:4(11):5775–81. https://doi.org/10.1021/am301557w

[15] Parrondo J, Wang Z, Jung MS, Ramani V. Reactive oxygen species accelerate degradation of anion exchange membranes based on polyphenylene oxide in alkaline environments. PCCP 2016:18:19705–12. doi.10.1039/C6CP01978A

[16] Park AM, Wycisk RJ, Ren X, Turley FE, Pintauro PN. Crosslinked poly(phenylene oxide)-based nanofiber composite membranes for alkaline fuel cells. J Mater Chem A 2016:4:132–141. doi.10.1039/C5TA06209H

[17] Zhang S, Zhang B, Zhao G, Jian X. Anion exchange membranes from brominated poly(aryl ether ketone) containing 3,5-dimethyl phthalazinone moieties for vanadium redox flow batteries, J Mater Chem A 2014;2:3083-91. Doi.10.1039/C3TA14503D

[18] Li X, Cheng S, Wang L, Long Q, Tao J, Nie G, Liao S. Anion exchange membranes by bromination of benzylmethyl-containing poly(arylene ether)s for alkaline membrane fuel cells. RSC Adv 2014;4:29682–93. doi.10.1039/C4RA00833B

[19] Nguyen MDT, Yang S, Kim D. Pendant dual sulfonated poly(arylene ether ketone) proton exchange membranes for fuel cell application. J Power Sour 2016;328:355–63. https://doi.org/10.1016/j.jpowsour.2016.08.041Get rights and content

[20] Li Z, Jiang Z, Tian H, Wang S, Zhang B, Cao Y, et al. Preparing alkaline anion exchange membrane with enhanced hydroxide conductivity via blending imidazolium-functionalized and sulfonated poly(ether ether ketone). J Power Sour 2015;288:384–92. https://doi.org/10.1016/j.jpowsour.2015.04.112

[21] Lee HC, Liu KL, Tsai LD, Lai JY, Chi-Yang Chao CY. Anion exchange membranes based on novel quaternized block copolymers for alkaline direct methanol fuel cells. RSC Adv 2014;4: 10944. doi.10.1039/C3RA47886F

[22] Liu L, He S.; Zhang, S.; Zhang, M.; Guiver MD, Li N.1,2,3-Triazolium-based poly (2,6-dimethyl phenylene oxide) copolymers as anion exchange membranes. ACS Appl Mater Interfaces 2016;8:4651–60. https://doi.org/10.1021/acsami.5b11519

[23] Patrick T. Nonjola, Mkhulu K. Mathe, Remegia M. Modibedi. Chemical modification of polysulfone: Composite anionic exchange membrane with TiO_2 nano-particles. Int J Hydrogen Energy 2013;38:5115 -21. https://doi.org/10.1016/j.ijhydene.2013.02.028

[24] Rajangam V, Muthukrishnan P, Dharmalingam S. Novel quaternized polysulfone/ZrO2 composite membranes for solid alkaline fuel cell applications. Int J. Hydrogen Energy 2011;36:7291-7302. https://doi.org/10.1016/j.ijhydene.2011.03.056

[25] Mohamad AA, Arof AK. Plasticized alkaline solid polymer electrolyte system. Mater Lett 2007;61:3096-99. https://doi.org/10.1016/j.matlet.2006.11.030

[26] Sang S, Zhang J, Wu Q, Liao Y. Influences of Bentonite on conductivity of composite solid alkaline polymer electrolyte PVA-Bentonite-KOH-H_2O. Electrochimica Acta 2007;52:7315-21. https://doi.org/10.1016/j.electacta.2007.06.004

[27] García-Cruz L, Casado-Coterillo C, Irabien A, Montiel V, Iniesta J, High Performance of Alkaline Anion-Exchange Membranes Based on Chitosan/Poly (vinyl) Alcohol Doped with Graphene Oxide for the Electrooxidation of Primary Alcohols. C 2016;2(2):10. https://doi.org/10.3390/c2020010

[28] Li Y, Shi S, Cao H, Zhao Z, Wen H. Modification and properties characterization of heterogeneous anion exchange membranes by electrodeposition of graphene oxide (GO), Appl Surf Sci 2018;442:700–10. https://doi.org/10.1016/j.apsusc.2018.02.166

[29] Jang SC, Chuang FS, Tsen WC, TKuo TW. Quaternized chitosan/functionalized carbon nanotubes composite anion exchange membranes, J Appl Polym Sci 2019. doi: 10.1002/APP.47778

[30] Movil O, Frank L, Staser JA. Graphene Oxide–Polymer Nanocomposite Anion-Exchange Membranes, J Electrochem Soc 2015;162(4):F419-F426. doi: 10.1149/2.0681504jes

[31] Kumar P, Bharti RP, Kumar V, Kundu PP. Polymer Electrolyte Membranes for Microbial Fuel Cells: Part A. Nafion-Based Membranes. Progress and Recent Trends in Microbial Fuel Cells 2018;4:47–72. doi:10.1016/b978-0-444-64017-8.00004-x

[32] Zheng Y, Ash U, Pandey RP, Ozioko AG, Ponce-Gonzalez J, Handl M, et al. Water Uptake Study of Anion Exchange Membranes, Macromolecules 2018;51:3264−78. https://doi.org/10.1021/acs.macromol.8b00034

[33] Mandal M, Huang G, Kohl PA. Highly Conductive Anion-Exchange Membranes Based on Cross-Linked Poly(norbornene): Vinyl Addition Polymerization, ACS Appl. Energy Mater 2019;2(4):2447-57. https://doi.org/10.1021/acsaem.8b02051

[34] Ion-Ebrasu D, Pollet BG, Spinu-Zaulet A, Soare A, Carcadea E, Varlam M, et al. Graphene modified fluorinated cation-exchange membranes for proton exchange membrane water electrolysis, Int J Hydrogen Energy 2019;44:10190-96. https://doi.org/10.1016/j.ijhydene.2019.02.148

[35] Sone Y, Ekdunge P, Simonsson D. Proton Conductivily of Nafion 117 as Measured by a Four-Electrode AC Impedance Method. J Electrochem Soc 1996;143(4):1254-1259. doi: 10.1149/1.1836625

[36] Vandiver MA, Caire BR, Carver JR, Waldrop K, Hibbs MR, Varcoe JR, et al. Mechanical Characterization of Anion Exchange Membranes by Extensional Rheology under Controlled Hydration. J Electrochem Soc 2014;161:H677-H683. doi:10.1149/2.0971410jes

[37] Aricò AS, Girolamo M, Siracusano S, Sebastian D, Baglio V, Schuster M. Polymer Electrolyte Membranes for Water Photo-Electrolysis, Membranes 2017;7,25: doi:10.3390/membranes7020025.

[38] Parthiban V, Akula S, Peera SG, Islam N, Sahu AK. Proton Conducting Nafion-Sulfonated Graphene Hybrid Membranes for Direct Methanol Fuel Cells with Reduced Methanol Crossover. Energy Fuels 2016;30:725−34. https://doi.org/10.1021/acs.energyfuels.5b02194

[39] Dong D, Zhang W, van Duin ACT, Bedrov D. Grotthuss versus Vehicular Transport of Hydroxide in Anion-Exchange Membranes: Insight from Combined Reactive and Nonreactive Molecular Simulations. J Phys Chem Lett, 2018;9(4):825–9. https://doi.org/10.1021/acs.jpclett.8b00004

[40] Bayer T, Cunning BV, Selyanchyn R, Daio T, Nishihara M, Fujikawa S, et al. Alkaline anion exchange membranes based on KOH-treated multilayer graphene oxide. J Membr Sci 2016;508: 51–61. https://doi.org/10.1016/j.memsci.2016.02.017

[41] Fang J, Qiao J, Wilkinson DP, Zhang J. Eds.,Electrochemical Polymer Electrolyte Membranes, 1st Edition; CRC Press Taylor & Francis Group 6000 Broken Sound Parkway NW, Suite 300 Boca Raton, Forida, USA, 2015; p. 365-448.

[42] Mohanapriya S, Bhat S, Sahu A, Manokaran A, Vijayakumar R, Pitchumani, S, et al. Sodium-alginate-based proton-exchange membranes as electrolytes for DMFCs. Energy Environ Sci 2010;3: 1746-56. doi.10.1039/C0EE00033G

[43] Li D, Yao J, Suna H, Liua B, Li D, van Agtmaal S, et al. Preparation and characterization of SiO2/PDMS/PVDF composite membrane for phenols recovery from coal gasification wastewater in pervaporation, Chem Eng Res Des 2018;1 3 2:424–35. https://doi.org/10.1016/j.cherd.2018.01.045

[44] Paul DK, McCreery R, Karan K. Proton Transport Property in Supported Nafion Nanothin Films by Electrochemical Impedance Spectroscopy. J Electrochem Soc 2014;161(14): F1395-402.

[45] Smith BC. Group Wavenumbers and an Introduction to the Spectroscopy of Benzene Rings. Spectroscopy 2016;31(3):34–7.

[46] Du X, Wang Z, Liu W, Xu J, Chen Z, Wang C. Imidazolium-functionalized poly (arylene ether ketone) cross-linked anion exchange membranes. J Membrane Sci 2018;566:205–12. https://doi.org/10.1016/j.memsci.2018.09.020

[47] Weiber EA, Meis D, Jannasch P. Anion conducting multiblock poly(arylene ether sulfone)s containing hydrophilic segments densely functionalized with quaternary ammonium groups. Polym Chem 2015;6, 1986-96. doi.10.1039/C4PY01588F.

[48] Tang L-C, Wan Y-J, Yan D, Pei Y-B, Zhao L, Li Y-B, et al. The effect of graphene dispersion on the mechanical properties of graphene/epoxy composites, Carbon 2013;60:16-27. https://doi.org/10.1016/j.carbon.2013.03.050

[49] Kartick B, Srivastava SK, Srivastava I. Green Synthesis of Graphene. J Nanosci Nanotechnol 2012;13:4320–24. doi:10.1166/jnn.2013.7461

[50] Menard KP, Dynamic Mechanical Analysis, A Practical Introduction, 2nd ed., CRC Press Taylor & Francis Group 6000 Broken Sound Parkway NW, Suite 300 Boca Raton, Forida, USA, 2008; pp. 33487-2742.